

AN OBSERVED CORRELATION BETWEEN THERMAL AND NON-THERMAL EMISSION IN GAMMA-RAY BURSTS

J. MICHAEL BURGESS^{1,2}, ROBERT D. PREECE^{1,2}, FELIX RYDE^{3,4}, PETER VERES⁵, PETER MÉSZÁROS⁵, VALERIE CONNAUGHTON², MICHAEL BRIGGS², ASAF PE'ER⁶, SHABNAM IYYANI^{4,3,7}, ADAM GOLDSTEIN⁸, MAGNUS AXELSSON^{9,3,4}, MATTHEW G. BARING¹⁰, P. N. BHAT², DAVID BYRNE¹¹, GERARD FITZPATRICK¹¹, SUZANNE FOLEY^{11,12}, DANIEL KOCEVSKI¹³, NICOLA OMODEI¹³, WILLIAM S. PACIESAS¹⁴, VERONIQUE PELASSA², CHRYSsa KOUVELIOTOU⁷, SHAOLIN XIONG², HOI-FUNG YU¹², BINBIN ZHANG², SYLVIA ZHU¹⁵

Draft version September 24, 2018

ABSTRACT

Recent observations by the *Fermi* Gamma-ray Space Telescope have confirmed the existence of thermal and non-thermal components in the prompt photon spectra of some Gamma-ray bursts (GRBs). Through an analysis of six bright Fermi GRBs, we have discovered a correlation between the observed photospheric and non-thermal γ -ray emission components of several GRBs using a physical model that has previously been shown to be a good fit to the Fermi data. From the spectral parameters of these fits we find that the characteristic energies, E_p and kT , of these two components are correlated via the relation $E_p \propto T^\alpha$ which varies from GRB to GRB. We present an interpretation in which the value of index α indicates whether the jet is dominated by kinetic or magnetic energy. To date, this jet composition parameter has been assumed in the modeling of GRB outflows rather than derived from the data.

Subject headings: gamma-ray burst: general — radiation mechanisms: non-thermal — radiation mechanisms: thermal

1. INTRODUCTION

Gamma-ray Bursts (GRBs) are believed to arise from the deaths of massive stars or the coalescence of two compact stellar objects such as neutron stars or black holes. The resulting explosion gives rise to an expanding fireball with a jet pointed at the observer but hidden from the observer until the density of radiation and particles in this highly relativistic outflow is low enough

for radiation to escape, a region called the photosphere (for a review see Mészáros 2006). While the emission from this fireball is expected to be thermal (Goodman 1986; Paczynski 1986), observations over the past three decades suggest the prompt emission to be highly non-thermal (Mazets et al. 1981; Fenimore et al. 1982; Matz et al. 1985; Kaneko et al. 2006; Goldstein et al. 2012), with only a few exceptions (Ryde et al. 2010; Ghirlanda et al. 2013). The conversion of the fireball energy into non-thermal γ -ray radiation involves the acceleration of electrons in the outflow and their subsequent cooling via an emission process such as synchrotron radiation (Sari et al. 1998; Tavani 1996). Insight into these energy radiation emission processes in GRBs is obtained by comparing the observed γ -ray photon spectra directly to different radiation models. The *Fermi* Gamma-ray Space Telescope offers a broad energy range for these comparisons. Recent observations (Guiriec et al. 2010; Zhang et al. 2011; Axelsson et al. 2012; Guiriec et al. 2013; Iyyani et al. 2013; Preece et al. 2014; Burgess et al. 2014) show that at least two mechanisms can be present: a non-thermal component that is consistent with synchrotron emission from accelerated electrons in the jet and a typically smaller blackbody contribution from the photosphere. This photospheric emission is released when the fireball becomes optically thin so that an observer may see a mixture of thermal and non-thermal emission with different temporal characteristics that, when viewed together, can probe the development and structure of the fireball jet. This simple photospheric model has been used to quantitatively interpret several observed correlations such as the Amati correlation (e.g., Thompson et al. 2007; Lazzati et al. 2011; Fan et al. 2012)

We are thus motivated to investigate correlations among spectral parameters derived by fitting the

¹ Department of Space Science, University of Alabama in Huntsville, Huntsville, AL 35899, USA:

jmichaelburgess@gmail.com, rob.preece@nasa.gov

² Center for Space Plasma and Aeronomic Research (CSPAR), University of Alabama in Huntsville, Huntsville, AL 35899, USA

³ Department of Physics, Royal Institute of Technology (KTH), AlbaNova, SE-106 91 Stockholm, Sweden: felix@particle.kth.se

⁴ The Oskar Klein Centre for Cosmoparticle Physics, AlbaNova, SE-106 91 Stockholm, Sweden

⁵ Department of Astronomy and Astrophysics, Pennsylvania State University, University Park, PA 16802, USA:

veres@gwu.edu, npp@astro.psu.edu

⁶ Physics Department, University College Cork, Cork, Ireland

⁷ Department of Physics, Stockholm University, AlbaNova, SE-106 91 Stockholm, Sweden

⁸ Space Science Office, VP62, NASA/Marshall Space Flight Center, Huntsville, AL 35812, USA

⁹ Department of Astronomy, Stockholm University, SE-106 91 Stockholm, Sweden

¹⁰ Rice University, Department of Physics and Astronomy, MS-108, P. O. Box 1892, Houston, TX 77251, USA

¹¹ University College Dublin, Belfield, Dublin 4, Ireland

¹² Max-Planck-Institut für extraterrestrische Physik (Giessenbachstrasse 1, 85748 Garching, Germany)

¹³ W. W. Hansen Experimental Physics Laboratory, Kavli Institute for Particle Astrophysics and Cosmology, Department of Physics and SLAC National Accelerator Laboratory, Stanford University, Stanford, CA 94305, USA

¹⁴ Universities Space Research Association, Huntsville, AL 35805, USA

¹⁵ Department of Physics and Department of Astronomy, University of Maryland, College Park, MD 20742, USA

non-thermal component with a synchrotron photon model and the thermal component with a blackbody, an approach developed in previous investigations (Burgess et al. 2012, 2014). The synchrotron model consists of an accelerated electron distribution, containing a relativistic Maxwellian and a high-energy power law tail that is convolved with the standard synchrotron kernel (Burgess et al. 2014, 2012; Rybicki & Lightman 1979). We find that the characteristic energies (E_p for synchrotron and kT for the blackbody) of the synchrotron and blackbody components are highly correlated across all the GRBs in our sample. We show that this correlation can be used to address the key question of how the energy of the outflow is distributed, i.e., whether the energy is in a magnetic field or is imparted as kinetic energy to baryons in the jet, and how this energy distribution evolves with time.

2. OBSERVATIONS

The *Fermi* Gamma-ray Burst Monitor (GBM) (Meegan et al. 2009) has detected more than 1200 GRBs since the start of operations on 2008, July 14. A smaller number have been seen by the *Fermi* Large Area Telescope (LAT) (Atwood et al. 2009) at energies greater than 100 MeV, but these are particularly interesting because they are among the brightest GRBs and offer the greatest opportunity for spectral analysis across a broad energy range. GRBs can last from a few milliseconds to hundreds of seconds or longer and have a variety of temporal profiles, from single spikes to multi-episodic overlapping pulses. Single-pulse GRBs exhibit the simplest spectral evolution, providing the “cleanest” signal for fitting physical models to the data (Burgess et al. 2014, 2012; Ryde & Pe’er 2009).

In this work, we analyze six bright, single-pulse GRBs detected by *Fermi* (see Table 1 and Figure 1) and find correlations between the E_p and kT values within each of these GRBs. The GRBs in our sample are GRB 081224A (Wilson-Hodge et al. 2008), GRB 090719A (van der Horst 2009), GRB 100707A (Wilson-Hodge et al. 2010), GRB 110721A (Tierney et al. 2011), GRB 110920A, GRB 130427A (von Kienlin 2013). The time histories of these GRBs are shown in Figure 1, with vertical dotted lines indicating the time binning used for the analysis of the spectral evolution of each spectral component. In a previous analysis (Burgess et al. 2014), the viability of fitting physical models to the *Fermi* GRB data was demonstrated for several GRBs and the spectral evolution of these models over the burst durations was investigated. The synchrotron model of Burgess et al. (2014), was constructed by convolving a shock-accelerated electron distribution of the form

$$n_e(\gamma) = n_0 \left[\left(\frac{\gamma}{\gamma_{\text{th}}} \right)^2 e^{-\gamma/\gamma_{\text{th}}} + \epsilon \left(\frac{\gamma}{\gamma_{\text{th}}} \right)^{-\delta} \Theta \left(\frac{\gamma}{\gamma_{\text{min}}} \right) \right] \quad (1)$$

with the standard synchrotron kernel (Rybicki & Lightman 1979). Here, n_0 normalizes the distribution to total number or energy, γ is the electron Lorentz factor in the fluid frame, γ_{th} is the thermal electron Lorentz factor, γ_{min} is the minimum electron Lorentz factor of the power-law tail, ϵ is the normalization of the power-law, and δ is the electron

spectral index. The function $\Theta(x)$ is a step function where $\Theta(x) = 0$ for $x < 1$ and $\Theta(x) = 1$ for $x > 1$. After convolution with the synchrotron kernel, the final fit parameters are the overall normalization of the spectrum, the νF_ν peak of the spectrum (E_p), and the electron spectral index, δ . These fits were found to be as good as those made with the empirical Band function (Band et al. 1993) that is the common choice for GRB spectroscopy. However, the Band function, being empirical, makes it difficult to deduce a more physical understanding. The fits with synchrotron model provide a direct association of the observed spectrum with a physical emission mechanism and therefore the fit parameters can be used to study properties of the GRB jet without ambiguity.

All of these GRBs were shown to be consistent with a physical model containing both a synchrotron and a blackbody component. For five of those GRBs we investigate herein correlations between the previously derived E_p and kT values, and we add to our sample the first pulse of the ultra-bright burst, GRB 130427A, for which a similar analysis has been performed (Preece et al. 2014). GRB 130427A is the brightest GRB detected by *Fermi* to date. Although its temporal structure is complex (Ackermann et al. 2014), it begins with a bright single pulse that is ideal for our physical modeling, which was used to show that internal shocks cannot explain the observed emission (Preece et al. 2014). GRB 081224A, GRB 110721A, and GRB 130427A were analyzed with GBM and LAT data; the rest of the sample were analyzed with GBM data alone. While this sample is limited by the number of bright, single-pulsed GRBs in the *Fermi* data set, this requirement allows reliable interpretation of the fits without confusion from overlapping pulses with different underlying spectra, which is essential to measuring the evolution of the thermal and non-thermal components throughout the duration of the GRB.

3. A CORRELATION BETWEEN SPECTRAL COMPONENTS

Figure 2 shows an example of the spectral evolution of the two separate components. A strong correlation is found between E_p and kT , as illustrated in Figures 3 & 4. A power law of the form $E_p \propto T^\alpha$ was fit to the E_p , kT pairs of the individual GRBs yielding values of α ranging from ~ 1 to 2 (see Table 1). The general temporal trend of both E_p and kT is an evolution from higher to lower energies. As can be seen from Figure 2, the evolution of the flux of each component is not necessarily tied to the change in the characteristic energies. This is very evident during the rise phase of a pulse during which the flux rises while E_p and kT fall with time. However, during the decay phase of the pulse, the flux decreases along with the characteristic energies. Table 1 lists the ratio of the blackbody flux to the total flux for each burst.

4. INTERPRETATION

To interpret these observations, we assume an emission process in which the thermal and non-thermal emission occur in close proximity to one another with the non-thermal synchrotron emission arising in an optically thin region above the photosphere of the jet. The range of the indices observed in the correlation suggests that the relation between the thermal and non-thermal emission

varies from burst to burst. One way to achieve this is to assume that the composition of GRB outflows vary in their ratio of magnetic content from being magnetically to baryonically dominated. In this scenario, the jet dynamics are parameterized by the dependence of the bulk Lorentz factor on the radius as $\Gamma \propto R^\mu$, from its initial launching radius of r_0 until the jet reaches its coasting Lorentz factor $\eta = L/\dot{M}c^2$ at the so-called saturation radius r_s , where L is the luminosity and \dot{M} is the mass outflow rate. This will be approximately the jet's Lorentz factor until it is decelerated upon collision with the surrounding medium. For magnetically-dominated jets $\mu \approx 1/3$ (Drenkhahn 2002; Drenkhahn & Spruit 2002; Kirk & Skjæraasen 2003), and in the baryonic case $\mu \approx 1$ (Mészáros et al. 1993). Intermediate values correspond to a mix of these components (Veres et al. 2013), and can be further modified by factors such as the topology of the magnetic field.

Under these assumptions, there are two regions of interest for which we can define the radial evolution of the bulk Lorentz factor:

$$\Gamma(r) = \begin{cases} (r/r_0)^\mu & \text{if } r < r_{\text{sat}} \\ \eta & \text{if } r_{\text{sat}} < r \end{cases} \quad (2)$$

Here, $r_{\text{sat}} = r_0\eta^{1/\mu}$ and is clearly larger when the jet is magnetically dominated. The emission of the blackbody is assumed to originate at the photospheric radius (r_{ph}), where the optical depth of the jet drops to unity. Following Mészáros et al. (1993), the photospheric radius is

$$\frac{r_{\text{ph}}}{r_0} = \left(\frac{L\sigma_{\text{T}}}{8\pi m_{\text{p}}c^3 r_0} \right) \frac{1}{\eta\Gamma_{\text{ph}}^2} \quad (3)$$

where Γ_{ph} is the Lorentz factor of the outflow at r_{ph} . The value of Γ_{ph} depends on the magnetic content of the outflow; therefore, r_{ph} can take on two values,

$$\frac{r_{\text{ph}}}{r_0} = \eta_{\text{T}}^{1/\mu} \begin{cases} (\eta_{\text{T}}/\eta)^{1/(1+2\mu)} & \text{if } \eta > \eta_{\text{T}} \\ (\eta_{\text{T}}/\eta)^3 & \text{if } \eta < \eta_{\text{T}} \end{cases} \quad (4)$$

The introduction of the critical Lorentz factor,

$$\eta_{\text{T}} = \left(\frac{L\sigma_{\text{T}}}{8\pi m_{\text{p}}c^3 r_0} \right)^{\mu/(1+3\mu)} \quad (5)$$

provides an important discriminator for the location of the r_{ph} relative to r_s . Outflows with $\eta = \eta_{\text{T}}$ have their photospheres at the saturation radius. Typical observed Lorentz factors of GRBs derived via different methods indicate values of a few hundred (Lithwick & Sari 2001; Pe'er et al. 2007). In a magnetically dominated ($\mu = 1/3$) case, we have $\eta_{\text{T}} \simeq 150 L_{53}^{1/6} r_{0,7}^{-1/6}$. For physically relevant values of $L = 10^{53} L_{53}$ erg s $^{-1}$ and $r_0 = 10^7 r_{0,7}$ cm, η_{T} is low compared to observed values for η . Therefore, the photosphere is in the acceleration phase for a large segment of the parameter space. On the other hand, in baryonic cases ($\mu = 1$), $\eta_{\text{T}} \simeq 1900 L_{53}^{1/4} r_{0,7}^{-1/4}$, which is several orders of magnitude higher than observed Lorentz factors. Therefore, we assume that magnetically dominated jets have their photospheres in the acceleration phase and baryonically dominated jets have their photospheres in the coasting phase. With this crit-

ical assumption, we derive two cases for the behaviors of both E_{p} and kT .

Close above the photosphere, instabilities in the flow or magnetic field line reconnection can lead to mildly relativistic shocks and accelerate leptons, which in turn emit synchrotron radiation (Mészáros & Rees 2011; McKinney & Uzdensky 2011). The synchrotron peak energy is dependent on the baryon number density $n'_b(r) = L/(4\pi r^2 m_{\text{p}} c^3 \Gamma(r)\eta)$ and the magnetic field $B' \propto n'^{1/2}$. The peak synchrotron energy is: $E_{\text{p}} = (3q_e B'_{\text{ph}}/4\pi m_e c)\gamma_{e,\text{ph}}^2 \Gamma_{\text{ph}}$. From this expression we derive the following dependence on the input parameters:

$$E_{\text{p}} \propto \begin{cases} L^{\frac{3\mu-1}{4\mu+2}} \eta^{-\frac{3\mu-1}{4\mu+2}} r_0^{\frac{-5\mu}{4\mu+2}} & \text{if } \eta > \eta_{\text{T}} \\ L^{-1/2} \eta^3 & \text{if } \eta < \eta_{\text{T}}. \end{cases} \quad (6)$$

The acceleration of the jet is assumed to be adiabatic for $r < r_{\text{sat}}$, leading to a relation between the comoving temperature (T') and the comoving volume (V') of $T' \propto V'^{-1/3}$. Since the expansion is along the radial direction of the jet, we have $V' = d^3x' = \Gamma d^3x \equiv 4\pi\Gamma r^2 dr$. Using Equation 2 for $r < r_{\text{sat}}$, we can write $\Gamma \propto r^\mu$. Therefore, the comoving temperature of the sub-dominant thermal component depends on radius as $T' \propto r^{-(\frac{\mu+2}{3})}$. Above the saturation radius, the standard evolution of the temperature is $T' \propto r^{-2/3}$. At the launching radius (r_0) the temperature is $T_0 = (L/4\pi r_0^2 ac)^{1/4}$. Therefore, the observed temperature for the two scenarios is:

$$kT_{\text{obs}}(r_{\text{ph}}) \propto \begin{cases} L^{\frac{14\mu-5}{12(2\mu+1)}} \eta^{\frac{2-2\mu}{6\mu+3}} r_0^{\frac{-10\mu-1}{6(2\mu+1)}} & \text{if } \eta > \eta_{\text{T}} \\ L^{-5/12} \eta^{8/3} r_0^{1/6} & \text{if } \eta < \eta_{\text{T}}. \end{cases} \quad (7)$$

It is unclear whether the evolution of the photosphere's luminosity or Lorentz factor, or some combination of both, drives the evolution of E_{p} and kT . One natural assumption is that the evolution of the photosphere's luminosity results in the observed variations in E_{p} and T as a burst proceeds. Therefore, considering the two types of jets; magnetically dominated ($r_{\text{ph}} < r_s$) and kinetic dominated ($r_{\text{ph}} > r_s$) we have two possibilities for the values of α :

- in the magnetic case, considering the appropriate powers of L , we have $E_{\text{p}} \propto T^{\frac{6(3\mu-1)}{14\mu-5}}$. The exponent is singular at $\mu \approx 0.36$, but for values up to $\mu < 0.6$ (these are the values of μ for which the photosphere will occur in the acceleration phase) we are able to explain values of α from 2 down to 1.4
- in the kinetic (baryonic) case we have $E_{\text{p}} \propto T^{1.2}$. This is observed in some GRBs.

5. DISCUSSION

The analysis of GRBs in the framework of this model can indicate whether the photosphere is in the acceleration or coasting phase, which in turn can be translated to the composition of the jet. We find that for exponents close to 2 the jet dynamics are dominated by the magnetic field while exponents close to 1 indicate baryonic jets. In our sample of six GRBs observed with *Fermi*, the exponents α of the relation between the characteristic energies of non-thermal and thermal components (Table

1) span the range of possible values, showing that energy content of GRB jets ranges from being dominated by the magnetic field to being contained mostly in the kinetic energy of baryons in the jet. A possible validation of this interpretation would be the future measurement of polarization in GRBs which will allow for the direct determination of the magnetization of GRB jets (see for example Lundman, Pe'er, & Ryde 2013).

We note that the lack of a correlation between the ratio of the thermal flux to the total flux with the inferred magnetic content of the jet is puzzling (see Table 1). Naively, it is expected that a photosphere occurring deep in the acceleration phase of the outflow will have its thermal emission be much brighter than the non-thermal emission. A possible explanation for the weakness of the observed thermal component has been addressed by several authors (Zhang & Yan 2011; Hascöet, Daigne, & Mochkovitch 2013). These works consider the effect of the magnetization parameter ($\sigma = \frac{B^2}{4\pi\Gamma\rho c^2}$) on the intensity of the thermal component where ρ is the matter density of the outflow. For $\sigma \gg 1$, most of the jet internal energy remains in the advected magnetic field, reducing the intensity of the observed thermal component from the photosphere. Another possibility for ex-

plaining the lack of correlation of the thermal flux ratios to the different jet modes is to consider that if the non-thermal flux is due to synchrotron following reconnection events above the photosphere, the amount of reconnection may not be simply given by the amount of magnetic energy and by the radius, but may depend also on the degree of tangledness of the field at that radius. For reconnection one needs field lines of opposite polarity near each other, and if the degree of randomness is stochastic (as it probably is), this could introduce a randomness in the amount of non-thermal electrons accelerated as well as the synchrotron flux produced. However, time-dependent simulations of magnetically dominated outflows in GRBs are not advanced enough to accurately test these assumptions and therefore the reduced intensity of the thermal component is still open to interpretation.

The *Fermi* GBM collaboration acknowledges support for GBM development, operations and data analysis from NASA in the US and BMWi/DLR in Germany. We also thank the anonymous referee for very useful comments that aided in refining this work.

REFERENCES

- Ackermann, M. et al. 2014, *Science*, 343, 42
 Atwood, W. B. et al. 2009, *ApJ*, 697, 1071
 Axelsson, M. et al. 2012, *ApJ*, 757, L31
 Band, D. et al. 1993, *ApJ*, 413, 281
 Burgess, J. M. et al. 2012, *ApJ*, 741, 24
 Burgess, J. M. et al. 2014, *ApJ*, 784, 17
 Hascöet, R. Daigne, F. & Mochkovitch R. 2013, *A&A*, 551, A124
 Drenkhahn, G. 2002, *A&A*, 387, 714
 Drenkhahn, G. & Spruit, H.C. 2002, *A&A*, 391, 1141
 Fan, Y.-Z., Wei, D.-M., Zhang, F.-W., & Zhang, B.-B. 2012, *ApJL*, 755, L6
 Fenimore, E. et al. 1982, *Nature*, 297, 665
 Ghirlanda, G. et al. 2013, *MNRAS*, 432, 3237
 Giannios, D. & Spruit, H. 2007, *A&A*, 469, 1
 Goldstein, A. et al. 2012, *ApJS*, 199, 19
 Goodman, J. 1986, *ApJ*, 308, L47
 Guiriec, S. et al. 2010, *ApJL*, 727, L33
 Guriec, S. et al. 2013, *ApJ*, 770, 32
 Iyyani, S. et al. 2013, *MNRAS*, 433, 2739
 Kaneko, Y. et al. 2006, *ApJS*, 166, 298
 Kirk, J.G. & Skjæraasen, O. 2003, *ApJ*, 591, 366
 Lazzati, D., Morsony, B. J., & Begelman, M. C. 2011, *ApJ*, 732, 34
 Lithwick, Y. & Sari, R. 2001, *ApJ*, 555, 540
 Lundman, C., Pe'er, A., & Ryde, F. 2013, *MNRAS*, 428, 2430
 Matz, S. et al. 1985, *ApJ*, 288, L37
 Mazets, E. et al. 1981, *Nature*, 290, 378
 McKinney, J. C. & Uzdensky, D. A. 2011, *MNRAS*, 1766, 1011.1904
 Meegan, C. et al. 2009, *ApJ*, 702, 791
 Mészáros, P. 2006, *Reports on Progress in Physics*, 69, 2259
 Mészáros, P., Laguna, P., & Rees, M. J. 1993, *ApJ*, 415, 181
 Mészáros, P. & Rees, M. J. 2011, *ApJ*, 733, L40
 Paczynski, B. 1986, *ApJ*, 308, L43
 Pe'er, A. et al. 2007, *ApJL*, 667, L1
 Preece, R. D. et al. 2014, *Science*, 343, 51
 Rybicki, M. J. & Lightman, A. 1979, *Radiative Processes in Astrophysics* (New York: Wiley and Sons)
 Ryde, F. & Pe'er, A. 2009, *ApJ*, 702, 1211
 Ryde, F. et al. 2010, *ApJ*, 709, L172
 Sari, R., Piran, T., & Narayan, R. 1998, *ApJ*, 497, L17
 Scargle, J., Norris, J., Jackson, B., & Chiang, J. 2013, *ApJ*, 764, 167
 Tavani, M. 1996, *ApJ*, 466, 768
 Tierney, D. et al. 2011, *GCN Circulars*, 12187
 Thompson, C., Mészáros, P., & Rees, M. J. 2007, *ApJ*, 666, 1012
 van der Horst, A. 2009, *GCN Circulars*, 9693
 Veres, P., Zhang, B. B., & Mészáros, P. 2013, *ApJ*, 764, 94
 von Kienlin, A. 2013, *GCN Circulars*, 14473
 Wilson-Hodge, C. et al. 2008, *GCN Circular*, 8723
 Wilson-Hodge, C. et al. 2010, *GCN Circular*, 10944
 Zhang, B. & Yan, H. 2011, *ApJ*, 726, 90
 Zhang, B.-B., Zhang, B., Liang, E.-W., et al. 2011, *ApJ*, 730, 141

GRB Name	α	Jet Type	μ	F_{BB}/F_{tot}
GRB 081224A	1.01 ± 0.14	baryonic	—	0.29
GRB 090719A	2.33 ± 0.27	magnetic	0.39 ± 0.01	0.27
GRB 100707A	1.77 ± 0.07	magnetic	0.42 ± 0.01	0.33
GRB 110721A	1.24 ± 0.11	baryonic	—	0.01
GRB 110920A	1.97 ± 0.11	magnetic	0.4 ± 0.01	0.39
GRB 130427A	1.02 ± 0.05	baryonic	—	0.22

TABLE 1

INDICES (α) AND DERIVED LORENTZ FACTOR RADIAL INDICES (μ) FROM FITTING POWER LAWS TO THE E_p , kT PAIRS FOR EACH GRB. THE INFERRED JET TYPE AND BLACKBODY (F_{BB}) TO TOTAL FLUX (F_{tot}) RATIOS ARE ALSO GIVEN. THE VALUES OF α FOR THE GRBS VARY BUT ARE WITHIN THE CONSTRAINTS OF THE MODEL DERIVED VIA OUR INTERPRETATION. VALUES OF μ ARE LISTED ONLY FOR THOSE GRBS THAT ARE INFERRED TO BE MAGNETICALLY DOMINATED. NO SIGNIFICANT CORRELATION BETWEEN α AND THE FLUX RATIOS WAS FOUND IN THE DATA.

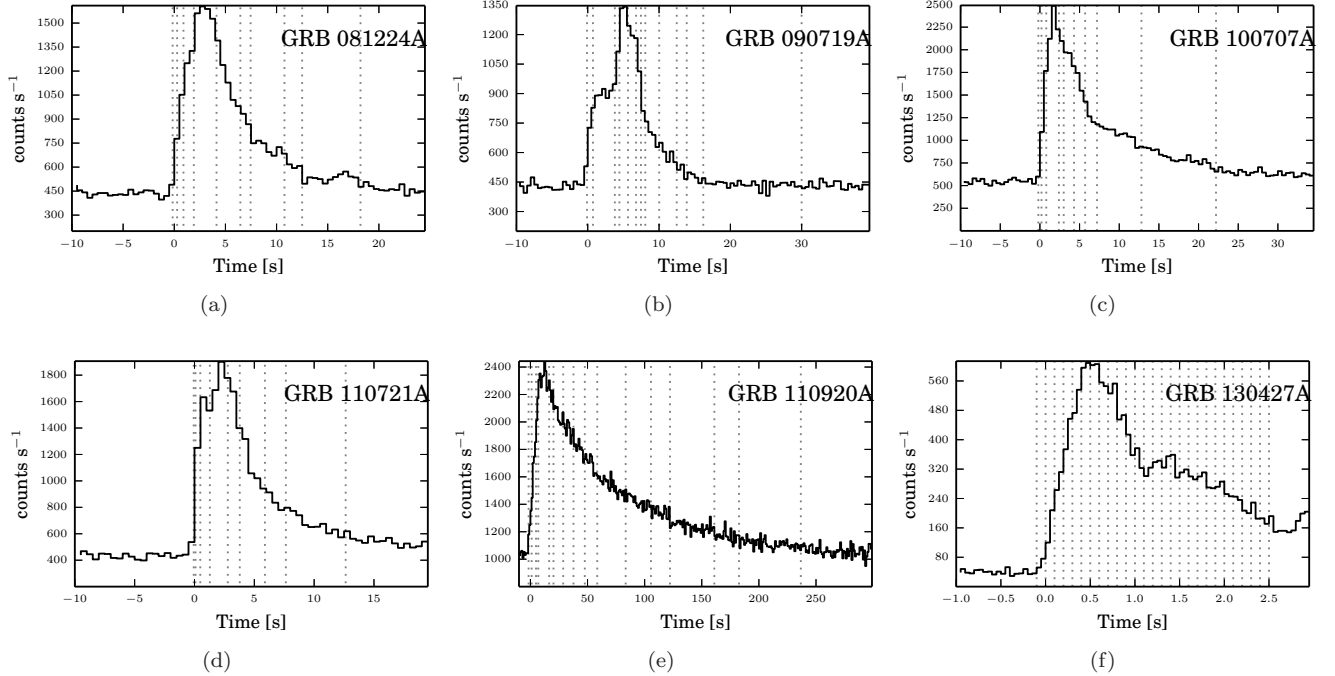


FIG. 1.— Each of the lightcurves in (a)-(f) shows the count rates detected by *Fermi* GBM for a GRB in our sample. The panels show the Sodium Iodide detector count rates between 8 and 300 keV. For each GRB in the sample, the time binning was selected by a Bayesian blocks algorithm (Scargle et al. 2013; Burgess et al. 2014) which operates by searching for significant changes in the count intensity. The bin selections are indicated by the vertical dotted lines.

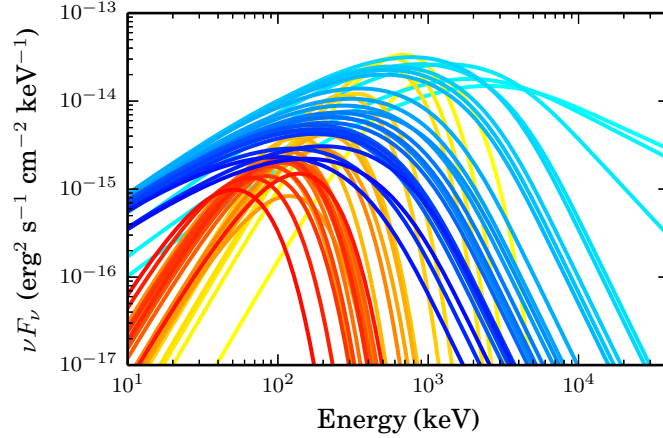


FIG. 2.— The νF_ν time-resolved spectrum of GRB 130427A (Preece et al. 2014). The evolution of the synchrotron component evolves from cyan to blue while the blackbody component evolution is shown from yellow to red with the time bins corresponding to Figure 1 (f). The correlation of E_p and kT is not obvious from the spectrum alone. Clearly the fluxes of the two components are not correlated.

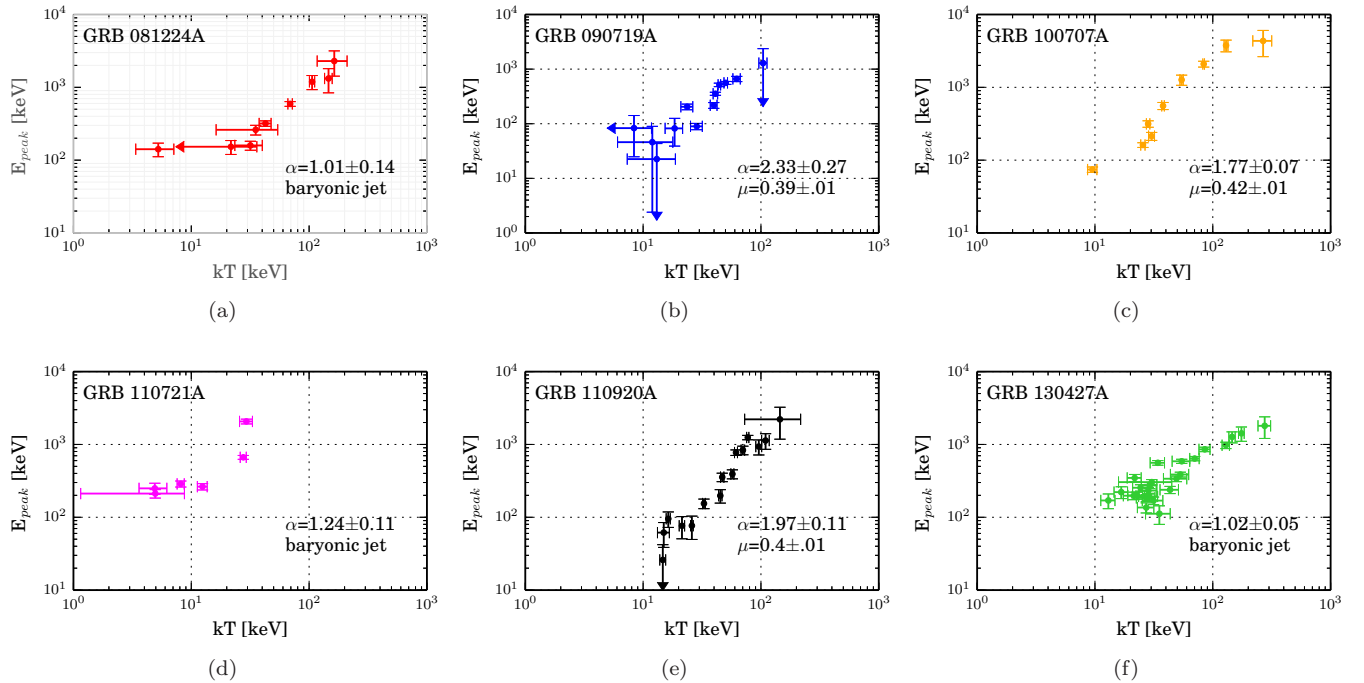


FIG. 3.— The individual observer frame correlations of each GRB all follow an observational relation of $E_p \propto T^\alpha$ where α ranges from $\sim 1 - 2$. At low E_p and kT , the characteristic energies are less well-constrained in the weaker tails of some of the GRBs. The relatively fewer data points for GRB 110721A (panel (d)) make the correlation difficult to measure.

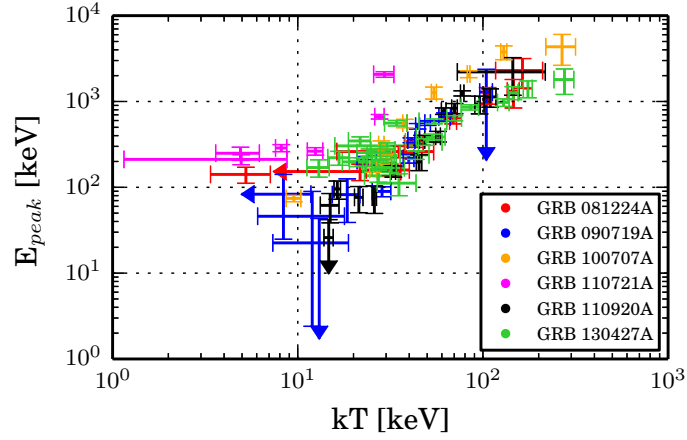


FIG. 4.— The time-resolved, observer-frame synchrotron and blackbody characteristic energies of the entire GRB sample. While the individual correlation index is not universal from burst to burst, it is clear that there is a strong correlation across the population. The Spearman rank correlation index, ρ , for the entire sample is 0.81 with a p-value of 4.35×10^{-20} .